frontiers | Frontiers in Sensors

TYPE Perspective
PUBLISHED 30 October 2025
DOI 10.3389/fsens.2025.1599365



OPEN ACCESS

EDITED BY
Alberto Quaranta,
University of Trento, Italy

REVIEWED BY
Simona Giordanengo,
National Institute of Nuclear Physics of Turin, Italy
Benedikt Ludwig Bergmann,
Czech Technical University in Prague, Czechia

*CORRESPONDENCE
Massimo Minuti,
massimo.minuti@pi.infn.it

RECEIVED 24 March 2025
ACCEPTED 03 September 2025
PUBLISHED 30 October 2025

CITATION
Minuti M, Baldini L, Beccherle R, Bellazzini R, Bisht A, Boscardin M, Brez A, Bruschi P, Ceccanti M, Vignali MC, Frontini L, Gaioni L, Ali OH, Latronico L, Liberali V, Magazzù G, Manfreda A, Manghisoni M, Morsani F, Orsini L, Palini L, Rollins MP, Pinchera M, Piotto M, Profeti A, Prosperi P, Ratti L, Ria A, Ronchin S, Sgrò C, Silvestri S, Spandre G, Stabile A, Traversi G, Trucco G, Vasquez M and Zanardo D (2025) ASIX: Single-photon, energy resolved X-ray imaging with 50 $\mu$m hexagonal hybrid pixel. *Front. Sens.* 6:1599365.
doi: 10.3389/fsens.2025.1599365



# ASIX: Single-photon, energy resolved X-ray imaging with 50 $\mu$m hexagonal hybrid pixel

Massimo Minuti[1]*, Luca Baldini[1,2], Roberto Beccherle[1], Ronaldo Bellazzini[1], Ashish Bisht[3], Maurizio Boscardin[3], Alessandro Brez[1], Paolo Bruschi[4], Marco Ceccanti[1], Matteo Centis Vignali[3], Luca Frontini[1], Luigi Gaioni[1,5], Omar Hammad Ali[3], Luca Latronico[1], Valentino Liberali[1,6], Guido Magazzù[1], Alberto Manfreda[1], Massimo Manghisoni[1,5], Fabio Morsani[1], Leonardo Orsini[1], Luca Palini[1], Melissa Pesce Rollins[1], Michele Pinchera[1], Massimo Piotto[4], Alessandro Profeti[1], Paolo Prosperi[1], Lodovico Ratti[1,7], Andrea Ria[4], Sabina Ronchin[3,8], Carmelo Sgrò[1], Stefano Silvestri[1,2], Gloria Spandre[1], Alberto Stabile[1,6], Gianluca Traversi[1,5], Gabriella Trucco[1,6], Monica Vasquez[1] and Danny Zanardo[3]

[1]National Institute for Nuclear Physics (INFN), Frascati, Italy, [2]Department of Physics, University of Pisa, Pisa, Italy, [3]Fondazione Bruno Kessler (FBK), Trento, Italy, [4]Department of Information Engineering, University of Pisa, Pisa, Italy, [5]Department of Engineering and Applied Sciences, University of Bergamo, Bergamo, Italy, [6]Department of Physics, University of Milano, Milano, Italy, [7]Department of Electrical, Computer and Biomedical Engineering, University of Pavia, Pavia, Italy, [8]Trento Institute for Fundamental Physics and Applications, Trento, Italy

The Analog Spectral Imager for X-rays is a technology demonstrator of a small-pixel Hybrid Pixel Detector (HPD) designed for applications such as X-ray diffraction, synchrotron-based material science, and soft X-ray astrophysics requiring energy-resolved imaging. The ASIX architecture aims at mitigating the adverse effects of charge sharing, typical of small-pixel devices. In contrast to other frame-based photon counters or multi-threshold devices, ASIX employs, along with a 50 $\mu$m pixel, an ultra-low-noise (<30 $e^-$ ENC), fully analog, asynchronous, single-photon readout, targeting 10 $\mu$m spatial resolution and 350 eV FWHM at 8 keV within the same exposure. In 2025, we began developing a small scale (~5 × 5 mm$^2$) HPD coupling a 300 $\mu$m-thick, n-on-p, edgeless silicon sensor with 50 $\mu$m pixels arranged in a hexagonal pattern to a newly designed 65-nm CMOS readout ASIC, featuring single-photon readout and on-chip analog to digital conversion, with a target rate capability of $10^8$ $ph/s/cm^2$. While the baseline for the ASIX R&D sensor is silicon for ≤20 keV operation, the design of the readout ASIC is compatible with High-Z materials sensors, such as cadmium-telluride or gallium-arsenide, for higher energies X-rays imaging, enabling potential extension to biomedical and preclinical research. This paper describes the ASIX imager architecture and reports on the development and testing of two Minimum Viable Products (MVPs), developed by coupling XPOL-III, a readily available 180-nm CMOS readout ASIC, to a 300 $\mu$m thick silicon sensor with 50 $\mu$m pixels and to a 750 $\mu$m thick CdTe sensor with 100 $\mu$m pixels, respectively. The MVPs achieved estimated energy resolution of 780 eV

FWHM at 17.5 keV (CdTe), and 620 eV FWHM at 9.7 keV (silicon) and spatial resolution of 20 $\mu$m (CdTe) and 7 $\mu$m (silicon). These results confirm our preliminary models predicting the feasibility of simultaneous high energy and spatial resolution in such a small-pixel devices, thus securing the ASIX specifications. Finally, the paper highlights the technology gaps that ASIX would potentially fill in both terrestrial and space applications.

KEYWORDS

**hybrid pixel detectors, X-ray spectral imaging, sub-pixel resolution, charge sharing, ASIC**

## 1 Introduction

X-ray radiation is widely used for digital imaging in medical, industrial, scientific, cultural heritage, and security applications. The advent of highly integrated electronics has enabled the development of digital imaging devices that combine high-density pixel matrices with in-pixel intelligence, enabling precise energy discrimination during image acquisition. In X-ray imaging, energy discrimination not only enhances image quality by rejecting background noise but also supports advanced measurement techniques, such as those used to identify specific materials within a sample (Taguchi, 2013; Stein et al., 2023; Tortora et al., 2022). Achieving superior image quality requires balancing different detector capabilities, in particular spatial and energy resolution. Improvements in the spatial resolution of the detector, typically achieved by designing ever smaller pixels, are counterbalanced by charge-sharing issues that affect the performance of the detector for pixel size below 100 $\mu$m (Mathieson et al., 2002). Since their first implementations in the late 1970s, Hybrid-Pixel-Detectors (HPDs) based on VLSI readout ASICs have attracted the interest of researchers thanks to Moore's Law-driven increases in pixel capacity. A continuous increase in the number of functions integrated in the pixel cell was possible and particle sensing techniques gained a strong advantage in terms of signal-to-noise ratio, mainly due to the reduced capacitance at the front-end input node. This promising scenario motivated researchers to strive for detectors with higher spatial resolution and sensitivity. Significant efforts have led to the development of several sensor modules, some of which exhibit exceptional performance metrics. In particular, sensor modules such as the Medipix/Timepix (CERN, Llopart et al. (2022); Sriskaran et al. (2024)), EIGER (Dectris Inc., Radicci et al. (2012)), and PIXIE (Pixirad Imaging Counters Srl, INFN Spin-off, Bellazzini et al. (2013); Bellazzini et al. (2015)) have demonstrated outstanding capabilities. However, their energy and spatial resolution still limit the sensitivity of many of the measurement setups or equipment in which they are involved. In these devices, the output signal of the pixel amplifier is continuously compared with a global threshold, and the content of a dedicated counter is incremented whenever the signal crosses it, or alternatively, the amplitude of the signal is sampled by means of time-over-threshold techniques. In these architectures, imaging performance is inherently limited by electronic noise, threshold uniformity, and charge sharing issues. While these challenges can be mitigated to some extent by design-for-matching techniques and intelligent in-pixel charge summing schemes (Bellazzini et al., 2015; Sriskaran et al., 2024), they cannot be completely eliminated. For small-pixel devices, charge sharing remains the primary limiting factor for both energy and spatial resolution (Ballabriga et al., 2020).

The ASIX (Analog Spectral Imager for X-rays) R&D project is focused on developing a small-scale ($\sim 5 \times 5\ mm^2$) technology demonstrator aimed at overcoming fundamental limitations in HPDs used for X-ray spectral imaging. ASIX will incorporate 50 $\mu$m pixels in a hexagonal array with single-photon, ultra-low-noise analog readout (<30 $e^-$ ENC), capable of precisely sampling the full charge distribution generated by the X-ray photon absorption, thus enabling high spatial (10 $\mu$m) and energy resolution (350 eV FWHM at 8 keV) in a single measurement. Thanks to its targeted performance, ASIX has the potential to improve sensitivity in applications requiring precise determination of both the energy and position of detected X-ray photons. The following sections outline our approach and report initial results from the ASIX Minimum Viable Product (ASIX-MVP), a CNTT-funded project to develop an intermediate HPD prototype designed to validate preliminary models predicting the resolution performance envisioned for the ASIX demonstrator.

## 2 Hybrid pixel architecture for precise charge cluster reconstruction

In pixel detectors, charge sharing occurs when an incoming X-ray photon deposits charge that spreads across multiple adjacent pixels, making it difficult to assign the event to a single pixel. Traditionally, in photon counting detectors, charge sharing is considered a drawback because it degrades both energy resolution and positional accuracy by splitting charge among neighboring pixels (Delogu et al., 2023). In systems with analog readout, charge sharing is a key factor enabling sub-pixel resolution imaging, delivering higher precision as the average size of the charge cluster increases. Unfortunately, while the sensor's spatial resolution benefits from charge sharing, the energy resolution does not. Indeed, electronic noise comes into play, limiting the best achievable energy resolution. As the average cluster size increases, so does the uncertainty in the sum of the individual pixel signals (Dinapoli et al. (2014); Cartier et al. (2016)). It must be noted that it is always possible to filter data to limit the average cluster size, thus improving the final energy resolution. However, this filtering negatively affects the spatial resolution and the sensor's data production rate. As a matter of fact, pixel detector systems do not perform equally well in all this metrics, and a trade-off must be set by tuning the sensor specifications in terms of pixel size, electronic noise, and sensor thickness. In our design we combine a fine-pitch 50 $\mu$m pixel and an ultra-low-noise, fully analog readout with a self-triggering logic capable of identifying the pixel with the maximum charge and selecting it for readout along with its six neighbors (hexagonal matrix). With such detailed information available offline for

every single photon, we shape the charge cluster by comparing the seven-pixel charge content against a digital threshold set at the pixel's noise level, after which we reconstruct:

- the photon absorption point, estimated as the centroid (center of gravity) of the charge distribution;
- its energy, obtained by summing the charge within the cluster.

Given the ASIX's baseline specifications, namely, the 50 $\mu$m pixel size and 300 $\mu$m thick silicon sensor, this approach is expected to deliver simultaneous moderate sub-pixel resolution (10 $\mu$m) and energy resolved (350 $eV$, FWHM at 8 keV) X-ray imaging. A drawback of this charge-cluster reconstruction is the increased processing time per event. However, ASIX will counteract this side-effect by employing a highly parallelized architecture, distributing workload across multiple Analog-to-Digital-Converters (ADCs) integrated on chip with a density of ~$10^3$ $ADCs/cm^2$. This will allow simultaneous digitization of multiple clusters. The 65-nm CMOS technology, selected for the ASIX demonstrator, enables the implementation of a highly packed digital electronics in the output data path, leading to high-speed serialization and supporting a rate capability of up to $10^8$ $ph/s/cm^2$.

## 3 Minimum-viable-product implementation and early results

INFN and Fondazione Bruno Kessler, supported the ASIX-MVP project, which aimed to develop a Minimum-Viable-Product (MVP) for the ASIX demonstrator. The goal was to demonstrate the effectiveness of our preliminary models in predicting the performance of our sensor given the configuration in terms of pixel size, sensor material and thickness, and readout noise. The MVP builds upon XPOL-III, a large scale (~2 $cm^2$) readout ASIC, which was readily available at INFN together with a companion FPGA based Data Acquistion system (DAQ). XPOL-III was originally developed to be integrated at the core of space-borne X-ray telescopes dedicated to polarimetry measurement in the 2 keV–8 keV energy range (Minuti et al., 2023). It features a 304 × 352 pixel hexagonal matrix, comprising over a 100k channels each occupying a 50 × 43 $\mu m^2$ area. Pixels include a contact pad on its top metal layer, which connects to a low-noise spectroscopic chain consisting of a Charge-Sensing Amplifier (CSA) with 30 $ke^-$ input linear range, a shaper with 1 $\mu$s peaking time, and a self-triggering peak detector circuit. When a charge is detected at the CSA input pad, XPOL-III isolates a rectangular Region of Interest (ROI), selecting for readout the pixels that detected a significant charge (~300 $e^-$) plus a margin (configurable in the 1 to 16 pixels range). During the readout sequence, which is controlled by the DAQ electronics, the amplifier output of the pixels belonging the ROI are sequentially connected to an analog output pad for off-chip analog-to-digital conversion, thus enabling precise single-photon processing. Moreover, once the original signal has been acquired, the peak detectors are cleared and the same ROI is readout several times (up to 4, configurable) for pedestal evaluation. The "pedestals" ROIs are averaged and subtracted from the "signal" ROI onboard the FPGA on an event-by-event basis. This enables for continuos accurate compensation of the pixel output baseline drift across temperature and sensor bias variations. In our system, a personal computer, running a dedicated application software, receives ROIs containing the photon data one by one from the DAQ. Typically, each ROI contains data related to one single photon. For each of them, we extract the exact charge distribution by performing basic zero suppression, comparing the pixel signal *versus* a threshold which is an input parameter of our algorithm. We then estimate the cluster size, i.e., how many pixels detected a significant charge, compute the photon absorption point and its energy. In our analysis, we have set this clustering threshold down to a 1-sigma noise level and configured the online pedestal subtraction logic in the FPGA to average four pedestal ROIs. The rate capability of this readout ($10^3$ $ph/s/cm^2$), achieved with a minimal segmentation (~0.5 $ADCs/cm^2$), poses a significant limitation for the use cases targeted by ASIX. However, its pixel geometry and readout principle, namely, 50 $\mu$m hexagonal arrangement and analog readout, are fully compatible with ASIX. Combined with its good noise performance and response uniformity, these features made XPOL-III a suitable candidate for the MVP development.

Although our baseline sensor is a ~300 $\mu$m silicon, coupling the ASIX readout to sensors made of different materials and thicknesses would broaden the range of potential applications for the new device. With this in mind, ASIX-MVP was designed to exploit the versatility that is typical of hybrid pixel detectors.

In December 2024, we delivered two HPD variants:

- a 750 $\mu$m thick Cadmium-Telluride (CdTe) Schottky-type sensor with 100 $\mu$m pixels
- a 300 $\mu$m thick n-on-p Silicon (Si) sensor with 50 $\mu$m pixels

Both coupled to the same XPOL-III readout ASIC.

In the following subsections, we synthesize the ASIX MVPs basic properties evaluation process and its outcomes. The basic characteristics of the Si and CdTe hybrids are summarized in Table 1.

### 3.1 Detector assembly and initial test

Upon completion of assembly in late 2024, we installed the hybrids in a custom designed detector housing which provides light shielding and dry-air environment enabling the cooling down to −30 °C. This temperature control is particularly beneficial for long-exposure operations of these detectors. We then performed preliminary tests to evaluate sensors performance.

Our initial tests focused on evaluating the pixel noise. Pixel noise was estimated by analyzing the pedestal residuals of 100 pixels located at the sensor center; for each pixel, the standard deviation of the residuals was computed, and the mean of these values was taken as the representative noise level. This analysis revealed a slight difference between the CdTe and Si hybrids pixel's noise, yielding 60 $e^-$ and 70 $e^-$ ENC respectively. Although sensor leakage current typically impacts noise performance, in our case it appears

TABLE 1 Summary of the basic properties of the ASIX-MVP HPDs.

| Parameter | CdTe | Si |
|---|---|---|
| Number of pixels | 26 752 (152 × 176) | 107 008 (304 × 352) |
| Pixel pitch | 100 $\mu$m | 50 $\mu$m |
| Thickness | 750 $\mu$m | 275 $\mu$m |
| Shaping time | 1 $\mu$s | 1 $\mu$s |
| Pixel Noise (ENC) | 60 $e^-$ | 70 $e^-$ |
| Energy resolution (FWHM)[1] | 780 eV (at 17.5 keV) | 620 eV (at 9.7 keV) |
| Spatial resolution[2] | 20 $\mu$m | 7 $\mu$m |
| Full scale linear range (FSLR) | 130 keV | 110 keV |
| Minimum trigger threshold | ~1.5 k$eV$ (1% of FSLR) | ~1.0 k$eV$ (1% of FSLR) |

[1]FWHM measurements at Mo-$K_\alpha$ (17.4 keV) and Au-$L_\alpha$ (9.7 keV) as shown in Figure 2 and corrected for the excess noise contribution due to the online pedestal subtraction.
[2]X-ray source: X-ray, Ag (25 kV) for CdTe, Au (10 kV) for Si.

negligible. We observed no significant change in noise across a 50 °C operating temperature range, despite leakage current varying by several orders of magnitude. Since the overall noise performance remained within ± 10% of our original expectations, we decided to postpone further investigations on this matter.

## 3.2 Spatial resolution

As a first check of the imaging performance of our devices, we performed a basic analysis of the Huttner 18-lead test pattern image response. The Huttner test pattern is a standard phantom used for estimation of the resolving power of a detection system for X-ray imaging. It consists of a 50 $\mu$m thick lead foil with slits at ever increasing density. The resolving power of the imaging system can be roughly assessed by analyzing the transmission image acquired through the phantom. We complemented the Huttner test with the Edge-Spread-Function (ESF) analysis based on the slanted-edge technique (Samei et al., 1998). In this imaging setup, the CdTe and Si hybrids were illuminated using a silver (Ag) target X-ray tube operated at 25 kV and one with gold (Au) target operated at 10 kV, respectively. Specifically for the CdTe setup, the X-ray source configuration was chosen to avoid resolution degradation due to cadmium (Cd) fluorescence.

During the imaging performance evaluation test campaign, we formed the images binning the estimated photon absorption point onto a two-dimensional reticle with 15 $\mu$m × 15 $\mu$m for the CdTe and 10 $\mu$m × 10 $\mu$m virtual pixel for the silicon sensor module. We filtered data selecting events with up-to four pixels, which represents more than 90% of the total. We computed the absorption point by applying basic center-of-gravity calculation. This technique is very simple and suitable for ease integration into hardware. However, more advanced techniques, aiming at reconstructing the centroid of the charge distribution, have the potential to provide more accurate results thus delivering even higher resolution images. We plan to explore the impact of such techniques in the near future. For the purpose of this paper, results obtained with the center-of-gravity calculation are already satisfactory. For the CdTe sensor, we estimated the spatial resolution, by means of the slanted-edge technique, acquiring an image of the edge of a 500 $\mu$m thick tungsten (W) tile with ~0.06 rad inclination with respect to the pixel rows orientation. We analyzed the edge profile in a 100 × 40 pixels roi. We finally estimated a spatial resolution of approximately 20 $\mu$m, which was consistent with the 40% modulation at 10 lp/mm estimation performed by analyzing the intensity profile on the Huttner test image. Thanks to the much smaller pixel size, the Si sensor modules exhibit higher spatial resolution making our Huttner test pattern ineffective, showing nearly full modulation at the densest pattern (10 lp/mm). We analyzed the intensity profile of the ~0.02 rad inclination edge in a 100 × 40 pixels roi in a portion of the Huttner test pattern image as shown in Figure 1. We estimated a spatial resolution of 7 $\mu$m, corresponding to ~50% modulation at 30 lp/mm or up to 50 lp/mm at 10% modulation (Figure 1). We confirmed such measurement by analyzing the same W-tile edge as we have done evaluating the CdTe spatial resolution.

## 3.3 Energy resolution

We evaluated energy resolution FWHM by analyzing the characteristic fluorescence radiation emitted by high-purity samples. For the CdTe sensor, we collected Molybdenum $k$-lines fluorescence by illuminating a 99.9% pure Mo sample with a silver target X-ray tube operated at 25 kV. For the silicon sensor, we acquired the gold $L$-lines fluorescence spectrum emitted by a 99.9% pure Au sample. In both test cases, we obtained pulse-height distributions using data collected from a group of 100 pixels located at the center of each detector. We filtered data selecting only those events with only one pixel exceeding the 1-sigma noise-level threshold. It limits the analysis to roughly 10% of the collected photons. Figure 2 shows the spectra acquired after minimal equalization of the pixels' response function. We fitted data with independent Gaussian functions. The limited number of counts,

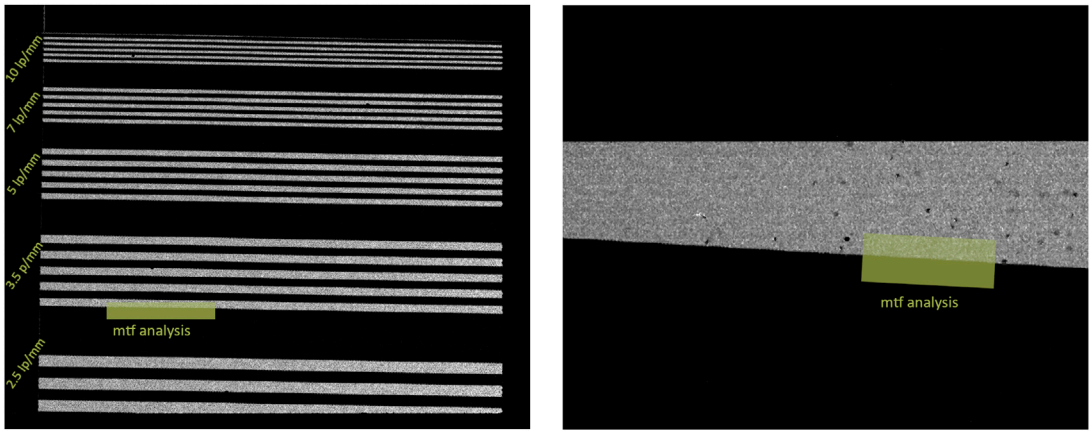


FIGURE 1
MVPs image data acquired for the evaluation of the spatial resolution (top), together with the MTF plots (bottom). For the silicon sensor (left), we analyzed the profile of a ~0.02 rad inclined edge in a 100 × 40 pixels ROI from the Huttner test pattern image acquired with 10 $\mu$m × 10 $\mu$m binning. For the CdTe sensor (right), we analyzed the profile of a ~0.06 rad inclined edge in a 100 × 40 pixels ROI from the Huttner test pattern image acquired with 15 $\mu$m × 15 $\mu$m binning. Images were formed by accumulating clusters up to four pixels in size.

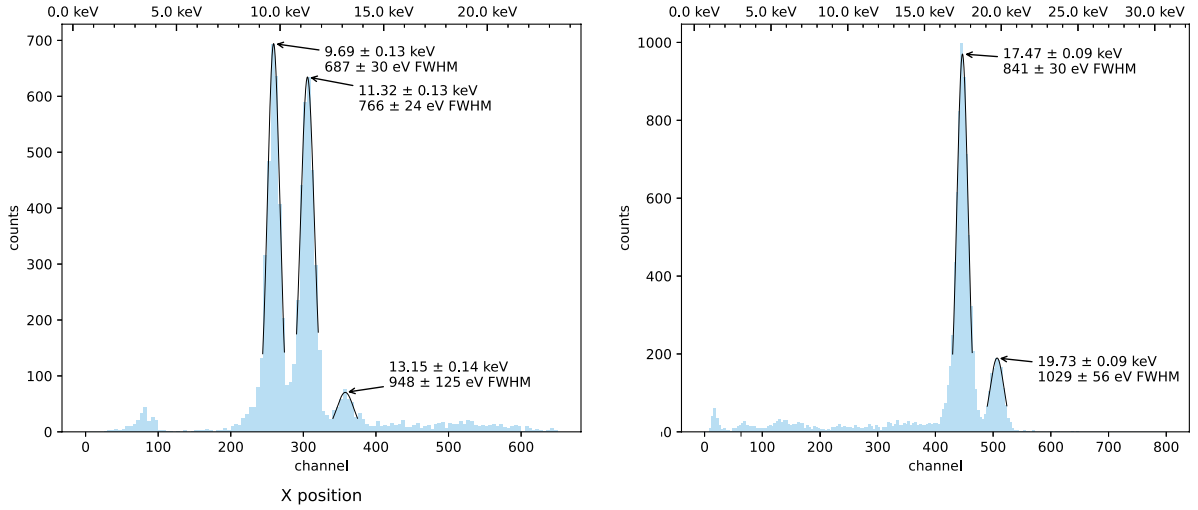


FIGURE 2
MVPs spectral data. (left) shows the Gold $L$-lines fluorescence spectrum ($L_{\alpha 1,2}$ 9.7 keV, $L_{\beta 1,2}$ 11.5 keV, $L_{\gamma 1}$ 13.4 keV) as recorded by the silicon sensor module. In this measurement we restricted the analysis to events with a one-pixel cluster size from a group of ~100 pixels at the center of the sensor's active area. (right) shows the Molybdenum $K$-lines fluorescence spectrum ($K_{\alpha 1,2}$ 17.4 keV, $K_{\beta 1-3}$ 19.6 keV) as recorded by the CdTe sensor module. The measured FWHM incorporates the excess electronic noise due to online pedestal subtraction, which we estimated to be roughly 300 eV FWHM for both sensor modules. The energy scale was calibrated by linear regression, incorporating Fe-55 calibration data (not shown) alongside the measured spectra.

registered in the low intensity peaks, determines the poor fitting accuracy. The latter, in conjunction with background effects which are related to the measurement setup, prevent us from focusing on those peak statistics for estimating the detector energy resolution. We postpone conducting deeper analysis on this topic to future measurements. Moreover, the presence of the $L_{\beta 1,2}$ doublet in the gold spectrum (11.4 keV), makes it not an ideal reference peak to estimate the detector performance. Energy resolution was then estimated at the Mo-$K_\alpha$ (17.4 keV) for the CdTe module and at the Au-$L_\alpha$ (9.7 keV) peak for the Si module. We emphasize that, in this measurement, due to the online pedestal subtraction, we are artificially introducing an excess noise contribution which we estimate to be half of the original electronic noise ($ENC/\sqrt{n}$, $n = 4$), yielding roughly 300 $eV$. The online pedestal subtraction is constrained by the DAQ electronics and is not mandatory for proper sensor operation. It could be replaced by a standard offline pedestal subtraction with negligible excess noise. Therefore, we estimate the sensors' intrinsic energy resolution by removing this excess noise from the FWHM measured at the main peaks of the spectra shown in Figure 2. With this in mind, we estimate an energy resolution of 780 ± 30 $eV$ (5% FWHM at 17.5 keV) and 620 ± 30 $eV$ (7% FWHM at 9.7 keV), for the CdTe

and the silicon sensor respectively. The CdTe sensor shows a degradation beyond the electronic noise limit (~670 eV), which we believe may be due to factors such as a drift in charge collection efficiency over the course of the data acquisition. Further investigation is planned, aiming to improve the outcomes of this measurement. On the other hand, for the Si sensor, the spread in the energy measurement is primarily dominated by the electronic noise.

# 4 Application outlook

Thanks to the fine pitch pixels, fully-analog event-driven readout, and targeted energy and spatial resolution, the ASIX's expected performance, combined with the versatility of hybrid pixel detectors, would offer several advantages over similar state-of-the-art detectors, opening the door to a wide range of applications that benefit from high-resolution effective single-photon processing. These applications can be broadly grouped into three main areas which we list in the following sub-sections.

## 4.1 Material science and analytical imaging

X-ray Diffraction analysis (XRD) is pivotal in material science, serving academia and industry. The market relies on XRD for detailed crystallographic, chemical, and physical material data. While typical 2-D XRD detectors provide good positional and angular resolution, they often lack energy resolution. In practice, most XRD equipment makes use of Copper (Cu) X-ray tubes which emit 8.048 keV $K_{\alpha 1}$, 8.029 keV $K_{\alpha 2}$, 8.905 keV Cu-$K_\beta$ radiation. Isolating the Cu-$K_\alpha$ radiation from the Cu-$K_\beta$ line is essential for achieving the best measurement accuracy. Current state-of-the-art pixel detectors do not have sufficiently good energy resolution to accomplish this task. As a result, passive k-edge absorption filtering is typically used (e.g., Nickel, 8.333 keV K-edge). However, passive filters introduce artifacts, due to the K-edge itself. They also attenuate the primary peak and still leave residual Cu-$K_\beta$ radiation. The ASIX approach addresses these limitations by offering:

- an efficient electronic "$K_\beta$ filter", eliminating the need for passive filtering;
- the option to exploit the monochromatic nature of the Cu-$K_\beta$ beam, electronically filtering out the Cu-$K_\alpha$, enabling more accurate analysis of complex data;
- improved rejection of fluorescence background.

Similarly, synchrotron-based material science experiments could benefit from the ASIX's performance, enhancing contrast in high-resolution imaging through improved background rejection.

## 4.2 Biomedical and preclinical research

ASIX would allow for more precise imaging of biological samples, revealing finer details and structures that lower resolution sensors cannot distinguish (Delogu et al., 2024; Feruglio et al., 2024; Christodoulou et al., 2024; Ballabriga et al., 2020). Specifically, it would enhance the sensitivity of equipment used in imaging techniques such as X-ray-Absorption-Spectroscopy (XAS) and K-edge Subtraction (KES), enabling better discrimination of different tissues based on their X-ray absorption characteristics. Moreover, ASIX would inherently provide a flexible platform for evaluating advanced data processing techniques, thereby contributing to the medical research community's efforts to improve the accuracy of diagnostic equipment.

## 4.3 Astrophysics and satellite remote sensing

X-ray telescopes typically employ focusing mirrors and a combination of CCD-based imaging and/or SDD-based spectroscopic detectors (e.g., Chandra, XMM, eRosita, eXTP/SFA) or, more recently, polarization sensitive gaseous detectors (e.g., PolarLight, IXPE, eXTP/PFA).

The ASIX technology is a natural, high-performance development of the focal plane detectors for future science missions. Next-generation X-ray observatories will require detectors with high quantum efficiency across the soft X-ray band to observe the faint objects that drive their mission science objectives. For example, Lynx, one of the four strategic mission concepts under study for the 2020 Astrophysics Decadal Survey, offers significant advances over previous and planned X-ray missions and provides synergistic observations in the 2030s to a multitude of space and ground-based observatories across all wavelengths (Gaskin et al., 2019). While purely speculative, it is worth noting the alignment between the envisaged performance of ASIX and the requirements of the Lynx-HDXI instrument (Hull et al., 2019), particularly in terms of resolving power in both the energy and spatial domains. Thanks to the inherently event-driven nature of its readout, ASIX offers a timing resolution of the order of 1 $\mu$s, enabling the simultaneous measurement of time, energy, and position for each detected photon. A boost in source sensitivity, which can potentially reduce observing times, can be envisaged thanks to the high throughput of the system and the possibility of tailoring the energy range to specific mission objectives.

Moreover, as the space business boasts new investments and opportunities, particularly pushed by cube-satellites and the growing interest in Earth Observations, new opportunities in the field of Space Weather and protection of infrastructures become available for the ASIX technology.

# 5 Discussion and conclusion

With the measured 7 $\mu$m spatial resolution and energy resolution (660 eV FWHM at 9.7 keV) limited by electronic noise in the 300 $\mu$m thick silicon sensor, the MVP data demonstrate the feasibility of achieving simultaneous high spatial and energy resolution using a small-pixel hybrid pixel detector, paving the way for the next phase of ASIX development. To fully qualify the technology, a new hybrid must be realized, one that integrates a redesigned readout ASIC tailored to the ASIX architecture. The upcoming ASIC will be engineered to meet stringent noise performance requirements (<30 $e^-$, ENC) while introducing a novel, parallel readout architecture based on multiple on-chip Analog-to-Digital Converters. This

enhancement will enable efficient cluster-based readout at high event rates (up to $10^8$ $ph/s/cm^2$ target).

In the long term, ASIX is envisioned as a scalable building block for large-area sensor matrices with minimal inactive regions. Its modular architecture ensures that expanded arrays can maintain high-resolution performance with manageable interconnect complexity, supporting deployment in advanced imaging systems across various domains. Over the next 2 years (2025–2026), the ASIX team will focus on developing this next-generation readout ASIC. In parallel, we will fabricate an edgeless silicon sensor using an innovative construction process built on top of that proposed by Koybasi et al. (2020), aimed at preserving wafer integrity without the use of a support wafer. These advancements will be key to transitioning ASIX from a promising demonstrator to a mature, deployable platform for high-performance X-ray spectral imaging. The ASIX project offers a novel approach to overcoming the long-standing trade-off between spatial and energy resolution in hybrid pixel detectors. By leveraging fine-pitch pixels, ultra-low-noise analog readout, and cluster-based reconstruction, ASIX will turn charge-sharing into an asset, enabling sub-pixel localization along with spectral fidelity. With its potential to deliver high-resolution, energy-resolved imaging, ASIX is well positioned to impact a wide range of applications, from materials analysis and biomedical imaging to astrophysics and remote sensing.

## Data availability statement

The datasets presented in this article are not readily available because the data is private. Requests to access the datasets should be directed to M. Minuti, minuti@infn.it.

## Author contributions

MMi: Writing – review and editing, Writing – original draft. LB: Writing – review and editing. RbB: Writing – review and editing. RnB: Writing – review and editing. AsB: Writing – review and editing. MB: Writing – review and editing. AlB: Writing – review and editing. PB: Writing – review and editing. MC: Writing – review and editing. MCV: Writing – review and editing. LF: Writing – review and editing. LG: Writing – review and editing. OH: Writing – review and editing. LL: Writing – review and editing. VL: Writing – review and editing. GM: Writing – review and editing. AM: Writing – review and editing. MMa: Writing – review and editing. FM: Writing – review and editing. LO: Writing – review and editing. LP: Writing – review and editing. MPR: Writing – review and editing. MiP: Writing – review and editing. MaP: Writing – review and editing. AP: Writing – review and editing. PP: Writing – review and editing. LR: Writing – review and editing. AR: Writing – review and editing. SR: Writing – review and editing. CS: Writing – review and editing. SS: Writing – review and editing. GS: Writing – review and editing. AS: Writing – review and editing. GiT: Writing – review and editing. GaT: Writing – review and editing. MV: Writing – review and editing. DZ: Writing – review and editing.

## Funding

The author(s) declare that financial support was received for the research and/or publication of this article. This work is funded by INFN CSN5, CSN2 and CNTT, the latter by means of the Research for Innovation (R4I) 2023 grant, and Fondazione Bruno Kessler.

## Acknowledgments

We would like to acknowledge our colleagues Raffaello D'Alessandro, Mirko Massi, and Mirko Brianzi from the Physics Department at University of Firenze and INFN for their invaluable support in the ASIX MVP hybrid assembly.

## Conflict of interest

The authors declare that the research was conducted in the absence of any commercial or financial relationships that could be construed as a potential conflict of interest.

## Generative AI statement

The author(s) declare that Generative AI was used in the creation of this manuscript to assist in refining the language of specific sections. All technical content, interpretation of data, and scientific conclusions were written and verified by the authors.

Any alternative text (alt text) provided alongside figures in this article has been generated by Frontiers with the support of artificial intelligence and reasonable efforts have been made to ensure accuracy, including review by the authors wherever possible. If you identify any issues, please contact us.

## Publisher's note



## References

Ballabriga, R., Alozy, J., Bandi, F. N., Campbell, M., Egidos, N., Fernandez-Tenllado, J. M., et al. (2020). Photon counting detectors for X-ray imaging with emphasis on CT. *IEEE Trans. Radiat. Plasma Med. Sci.* 5, 422–440. doi:10.1109/trpms.2020.3002949

Bellazzini, R., Spandre, G., Brez, A., Minuti, M., Pinchera, M., and Mozzo, P. (2013). Chromatic x-ray imaging with a fine pitch cdte sensor coupled to a large area photon counting pixel asic. *J. Instrum.* 8, C02028. doi:10.1088/1748-0221/8/02/C02028

Bellazzini, R., Brez, A., Spandre, G., Minuti, M., Pinchera, M., Delogu, P., et al. (2015). Pixie iii: a very large area photon-counting cmos pixel asic for sharp x-ray spectral imaging. *J. Instrum.* 10, C01032. doi:10.1088/.1748-0221/10/01/C01032

Cartier, S., Kagias, M., Bergamaschi, A., Wang, Z., Dinapoli, R., Mozzanica, A., et al. (2016). Micrometer-resolution imaging using MÖNCH: towards $G_2$-less grating interferometry. *J. Synchrotron Radiat.* 23, 1462–1473. doi:10.1107/S1600577516014788

Christodoulou, P., Alozy, J., Ballabriga, R., Campbell, M., Heijne, E., Llopart, X., et al. (2024). Probability distribution maps of deposited energy with sub-pixel resolution for timepix3 detectors. *J. Instrum.* 19, C01026. doi:10.1088/1748-0221/19/01/C01026

Delogu, P., Di Trapani, V., Golosio, B., Longo, R., Rigon, L., and Oliva, P. (2023). Characterization of charge sharing and fluorescence effects by multiple counts analysis in a pixie-ii based detection system. *Nucl. Instrum. Methods Phys. Res. Sect. A Accel. Spectrom. Detect. Assoc. Equip.* 1047, 167874. doi:10.1016/j.nima.2022.167874

Delogu, P., Biesuz, N., Bolzonella, R., Brombal, L., Cavallini, V., Brun, F., et al. (2024). Validation of timepix4 energy calibration procedures with synchrotron x-ray beams. *Nucl. Instrum. Methods Phys. Res. Sect. A Accel. Spectrom. Detect. Assoc. Equip.* 1068, 169716. doi:10.1016/j.nima.2024.169716

Dinapoli, R., Bergamaschi, A., Cartier, S., Greiffenberg, D., Johnson, I., Jungmann, J. H., et al. (2014). MÖNCH, a small pitch, integrating hybrid pixel detector for X-ray applications. *J. Instrum.* 9, C05015. doi:10.1088/1748-0221/.9/05/C05015

Feruglio, A., Biesuz, N., Bolzonella, V. R., Fiorini, M., Rosso, V., and Delogu, P. (2024). Timepix4 calibration and energy resolution evaluation with fluorescence photons. *Il Nuovo Cimento* 47-C. doi:10.1393/ncc/i2024-24314-6

Gaskin, J. A., Swartz, D., Vikhlinin, A. A., Özel, F., Gelmis, K. E. E., Arenberg, J. W., et al. (2019). Lynx X-Ray Observatory: an overview. *J. Astronomical Telesc. Instrum. Syst.* 5, 021001. doi:10.1117/1.JATIS.5.2.021001

Hull, S. V., Falcone, A. D., Bray, E., Wages, M., McQuaide, M., and Burrows, D. N. (2019). Hybrid CMOS detectors for the Lynx x-ray surveyor high definition x-ray imager. *J. Astronomical Telesc. Instrum. Syst.* 5, 021018. doi:10.1117/1.JATIS.5.2.021018

Koybasi, O., Zhang, J., Kok, A., Summanwar, A., Povoli, M., Breivik, L., et al. (2020). Edgeless silicon sensors fabricated without support wafer. *Nucl. Instrum. Methods Phys. Res. Sect. A Accel. Spectrom. Detect. Assoc. Equip.* 953, 163176. doi:10.1016/j.nima.2019.163176

Llopart, X., Alozy, J., Ballabriga, R., Campbell, M., Casanova, R., Gromov, V., et al. (2022). Timepix4, a large area pixel detector readout chip which can be tiled on 4 sides providing sub-200 ps timestamp binning. *J. Instrum.* 17, C01044. doi:10.1088/1748-0221/17/01/C01044

Mathieson, K., Passmore, M., Seller, P., Prydderch, M., O'Shea, V., Bates, R., et al. (2002). Charge sharing in silicon pixel detectors. *Nucl. Instrum. Methods Phys. Res. Sect. A Accel. Spectrom. Detect. Assoc. Equip.* 487, 113–122. doi:10.1016/S0168-9002(02)00954-3

Minuti, M., Baldini, L., Bellazzini, R., Brez, A., Ceccanti, M., Krummenacher, F., et al. (2023). Xpol-iii: a new-generation vlsi cmos asic for high-throughput x-ray polarimetry. *Nucl. Instrum. Methods Phys. Res. Sect. A Accel. Spectrom. Detect. Assoc. Equip.* 1046, 167674. doi:10.1016/j.nima.2022.167674

Radicci, V., Bergamaschi, A., Dinapoli, R., Greiffenberg, D., Henrich, B., Johnson, I., et al. (2012). Eiger a new single photon counting detector for x-ray applications: performance of the chip. *J. Instrum.* 7, C02019. doi:10.1088/1748-0221/7/02/C02019

Samei, E., Flynn, M. J., and Reimann, D. A. (1998). A method for measuring the presampled mtf of digital radiographic systems using an edge test device. *Med. Phys.* 25, 102–113. doi:10.1118/1.598165

Sriskaran, V., Alozy, J., Ballabriga, R., Campbell, M., Christodoulou, P., Heijne, E., et al. (2024). High-rate, high-resolution single photon x-ray imaging: Medipix4, a large 4-side buttable pixel readout chip with high granularity and spectroscopic capabilities. *J. Instrum.* 19, P02024. doi:10.1088/1748-0221/19/02/P02024

Stein, T., Rau, A., Russe, M. F., Arnold, P., Faby, S., Ulzheimer, S., et al. (2023). Photon-counting computed Tomography - basic principles, Potenzial benefits, and initial Clinical experience. *Rofo* 195, 691–698. doi:10.1055/a-2018-3396

Taguchi, K. I. J., and Iwanczyk, J. S. (2013). Vision 20/20: single photon counting x-ray detectors in medical imaging. *Med. Phys.* 40, 100901. doi:10.1118/1.4820371

Tortora, M., Gemini, L., D'Iglio, I., Ugga, L., Spadarella, G., and Cuocolo, R. (2022). Spectral photon-counting computed Tomography: a review on technical principles and Clinical applications. *J. Imaging* 8, 112. doi:10.3390/jimaging8040112